Eighth International Symposium on Marine Propulsors
smp'24, Berlin, Germany, March 2024

Design of unconventional Propellers for the HSVA Hamburg Container Ship (HCS)

Thomas Lücke[1]

[1]Hamburgische Schiffbau-Versuchsanstalt GmbH (HSVA), Hamburg, Germany

ABSTRACT

Within the national founded research project DeffProForm HSVA has designed two unconventional tip-rake propellers for the HSVA Hamburg Container Ship (HCS). This test case represents a 8000 TEU post-panmax container ship. The aim of the work was to investigate and to make full use of the potential provided by unconventional propeller designs aiming at reducing the fuel consumption by increasing the propeller efficiency. Therefore HSVA has enhanced the design procedure for such unconventional tip-rake propellers as well as the numerical tools (BEM-, RANS-code) for their performance prediction.

During the design process the potential of positive and negative rake orientation has been investigated regarding efficiency and cavitation characteristics. Focus has been set on differences between conventional and the unconventional blade shapes as well as the capability of the analysis tools to predict them.

For validation purpose of the new designs and the numerical tools, model tests have been performed in HSVA's large towing tank, conventional cavitation tunnel and the HYKAT.

This paper summarizes the design work, experience and investigations done at HSVA to achieve a better understanding and predictability of these kinds of unconventional propellers.

Keywords

Unconventional propeller design, tip-rake, efficiency, limiting stream lines, RANS, CFD

1 INTRODUCTION

When designing a ship propeller the focus on efficiency drives the design sometimes towards extreme shapes with possible drawbacks. Reducing the blade area ratio is one possibility which reduces the frictional drag and increases the propeller efficiency. Unconventional blade shapes as tip-rake propellers which reduce the induced drag gained much attention. Positive- as well as negative tip rake propeller design philosophies exist, for example propellers with negative tip-rake (Andersen et al. 2002) as well as positive tip-rake designs (Brown et al. 2014; Gaggero et al. 2015).

These tip-rake geometries allow extending the effective span by fixed propeller diameter and extending the degree of freedom to introduce further design and load parameters due to the non-planar shape of the tip-rake.

HSVA Hamburg Container Ship (HCS) Test case has been chosen as the design target (Schumacher 2020). The hull lines, rudder and the stock propeller are open for the public. All geometries will be prepared to be found on the HSVA home page www.hsva.de. Some particulars can be read off from Table 1.

Table 1: Ship Main Particulars

Lpp =	312.72 m	LOS =	325.94 m
B =	48.2 m	T_{design} =	13.0 m
PB_{MCR} =	42306 kW	CB =	0.6338
Dprop =	9.5 m	Scale =	38
n_{MCR} =	75 rpm	LRM =	5%

2 DESIGN - PROCEDURE

Extreme rake shapes ask for introducing additional design parameters, which are able to describe the blade geometry beyond the classical cylindrical coordinate system with constant radii. The latter is inappropriate to describe extreme tip-rake blades due to the non-planar tip shape. Similar as for KAPPEL propellers (Andersen et. al. 2002) introducing two additional profile orientation angles ϕ_u, ϕ_w seems to be an appropriate approach.

A local coordinate system is introduced in Cartesian coordinates, where the u-coordinate represents the local nose tail line at point of reference indicated by means of white vectors in Figure 1, whereas the local w-coordinate points orthogonal to the nose tail line within the pitch plane or x-y-plane, indicated by green vectors.

The angle ϕ_u rotates around the u-coordinate counting positive towards the face- or pressure side. By means of this angle the profile ordinates or the thickness can follow the orientation of the rake distribution. The angle ϕ_w rotates around the w-coordinate, positive leading edge down. A positive pitch angle ϕ_w introduces a load increase on the suction side of a strongly raked tip. Both additional angles allow adopting the blade shape while distributing the radial loading towards the tip.

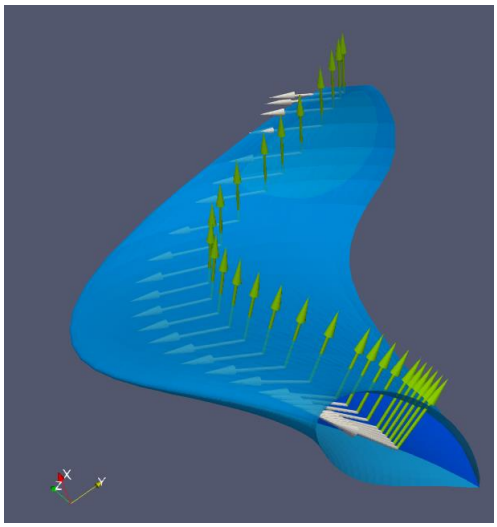

Figure 1: Perspective view onto the blade geometry showing the base vectors for aligning ϕ_u (white) and ϕ_w (green)

Still a radial instead of a span oriented coordinate system has been applied. Principally the nominal propeller diameter is valid only for the reference line.

2.1 Method of Analysis

The HSVA boundary element method (BEM) PPB (Streckwall, 2000) is able to handle a Cartesian blade description and was prone to be used for the designs and their subsequent analyses. Figure 2 shows the panel representation of both negative- and positive-rake blades. Especially in the tip region the grid density has been increased to be able to account for the local flow behavior.

The most practicable way for exchanging 3D CAD data and to serve for the link towards RANS predictions was to create an explicitly understandable Cartesian file format, which can be read in and processed within CAESES. Thanks to a macro the processing of the input file towards a clean CAD format became handy. Figure 3 shows exemplarily the geometry for propeller open water (POW) predictions by means of RANS.

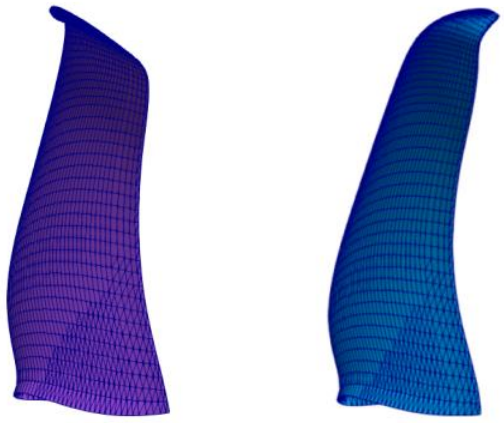

negative tip-rake positive tip-rake

Figure 2: Panel representation of two design propellers

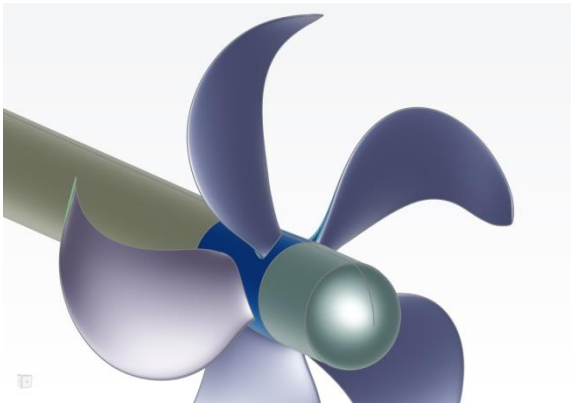

Figure 3: CAD-geometry for POW prediction

During the design process the blade shape defining analyses were performed with PPB within the wake field, balancing and optimizing the propulsion and the cavitation behavior. The propulsion predictions are performed by means of classical prognoses with stock propeller based constant propulsion coefficients (thrust deduction fraction t, effective wake fraction w and relative rotative efficiency η_R) and ship resistance R_T by changing only the POW characteristic for every propeller version determined by PPB. When the confidence was high enough, POW and propulsion analyses by means of a full RANS approach with FreSCo$^+$ were made.

FreSCo$^+$ is the HSVA in-house viscous flow solver (RANS solver) especially developed for marine applications (Hafermann, 2007). The flow is analyzed in full scale and is assumed to be fully turbulent. The k-ω shear stress transport (k-ω-SST) turbulence closure model has been applied. Wall-functions describe the velocity distribution of the turbulent flow regime by means of the universal log-law and estimate the flow variables in the viscous sub-layer.

Ship hull and rudder were placed in a stationary grid domain where the propeller was located within a rotating cylinder. Both domains communicate with each other by sliding interface technique. For the propellers in question only the cylindrical grid needed to be replaced. The time step for the transient analyses corresponded to $\omega*\Delta t=1°$. All results represent mean values out of the last complete propeller revolution within the transient analysis. To limit the effort for the propulsion prediction the free surface has been neglected by a double body approach.

The propulsion evaluation is performed by means of load variation with two propeller speeds at design ship speed. Between these results the thrust T, the torque Q, and the longitudinal hull force F_x have been interpolated linearly. Since the hull force and the corresponding resistance is not explicitly known by the double body approach (due to missing wave- and wind resistance), an artificial added hull force ΔF_x has been introduced in order to meet the appropriate propeller thrust. Since ΔF_x is not known in advance it is adjusted to meet the total resistance R_T from the resistance and propulsion tests conducted prior to the design phase.

$$R_T = T*(1-t) = (F_x + \Delta F_x)*(1-t) \quad (1)$$

The resistance R_T determined by resistance tests or CFD predictions is similar to the hull force under propulsion condition at zero propeller thrust T but usually smaller by a few percent. According to HSVA model test statistics the following relation holds for container vessels:

$$R_T \leq (F_x + \Delta F_x)_{,(T=0)} \quad (2)$$

$$R_T = (F_x + \Delta F_x)_{,(T=0)} / 1.044 \quad (3)$$

The above relation has been applied onto the actual CFD results to close the gap between $F_{x,(T=0)}$ and R_T. For the propeller shapes investigated ΔF_x has been adjusted individually to match R_T as a necessary propeller independent result.

2.2 Experience with Positive- and Negative Tip-Rake

Negative and positive tip-rake orientations were both investigated during this design work to evaluate their specific characteristics. Positive rake is defined as aftwards or towards the pressure side. By means of this design example, we would like to share the experience made so far.

In the present case positive tip-rake propeller versions showed slightly lesser efficiency gain versus negative tip-rake propellers.

For both propellers the strategy was to concentrate more loading towards the tip, as it is the idea behind this unconventional propeller concept. As a consequence the radial sheet cavitation extension and its time wise behaviour were aimed to be reduced towards fractions near the tip, which is able to create a stable sheet cavitation pattern and additional tip vortex behaviour w/o bursting pattern. Accounting these thoughts the blade area has been chosen smaller than of the stock propeller.

The idea was that the tip of the negative rake allows increasing the tip loading and in parallel shielding the cavitation-related pressure pulses at least partly from the hull. This shielding effect was not expected to come along with positive rake orientation.

For the positive tip-rake propellers the POW results of RANS and BEM methods were relatively close to each other, to the contrary of the negative tip-rake versions.

It turned out that the positive tip-rake orientation revealed a moderate sensitivity in terms of efficiency and cavitation due to applied geometrical changes. To the contrary the negative tip-rake geometries behaved more sensitive towards design variations. Positive tip-rake versions seem to forgive possible inappropriate design measures more than negative tip-raked ones.

3 RESULTS

Figure 4 shows a comparison of the radial distribution of the circumferential averaged bound circulation between the conventional stock propeller and unconventional propellers with negative- and positive tip-rake respectively. As aimed for, the radial loading of both unconventional propellers is much higher towards the tip, than for the conventional one.

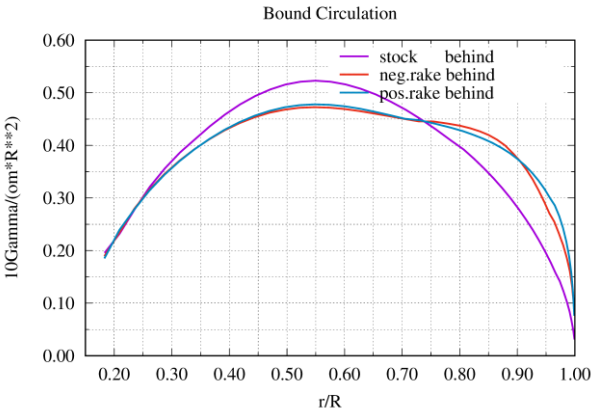

Figure 4: Bound circulation in behind condition

In Table 2 the propeller main particulars of the propellers are shown.

Table 2: Propeller Main Particulars

Propeller	**Stock**	**Pos-rake**	**Neg-rake**
type	conv.	un-conv.	un-conv.
D (m)	9.5	9.5	9.5
A_e/A_0	0.665	0.606	0.603
$t/c_{(0.7R)}$	0.050	0.073	0.076
P_m/D	1.044	1.062	1.082
Z	5	5	5

Exemplarily for several obtained results Figures 5 and 6 show the mean pressure distribution within the wake on the back side of positive- and negative tip-rake version respectively. The aforementioned low sensibility of the positive raked type can most probably be related to the moderate pressure distribution near the tip. To the contrary a lower pressure region near the tip of the negative tip-rake is present, which was more difficult to eliminate than for the positive tip-rake propellers.

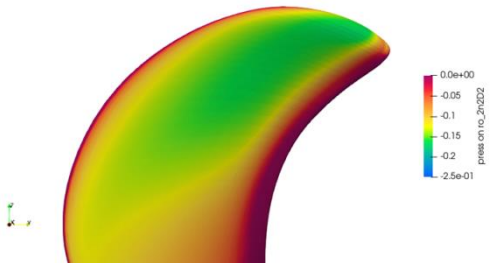

Figure 5: Cp-distribution on positive-rake design

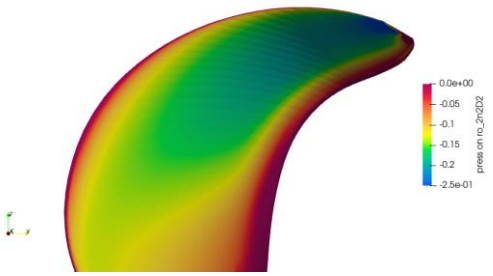

Figure 6: Cp-distribution on negative-rake design

Since a late cavitation inception speed is not the main goal of a container ship propeller, cavitation must not be classically reduced but the cavitation behaviour should be stabilized as much as possible. Low time-wise variations of the cavitation volume would lead to low pressure pulses and to low underwater radiated noise. The latter would be helpful for fulfilling noise regulations.

3.1 Propulsion Behavior

Figure 7 shows exemplarily the surface pressure distribution from the propulsion analysis by means of c_p-coefficient together with the limiting stream lines on the aft ship and on the back side of the negative tip-raked propeller. D represents the propeller diameter, n the propeller speed, ρ the water density, p the pressure and p_{ref} the reference pressure.

$$c_p = \frac{p - p_{ref}}{0.5\rho\,(\pi \cdot n \cdot D)^2} \qquad (4)$$

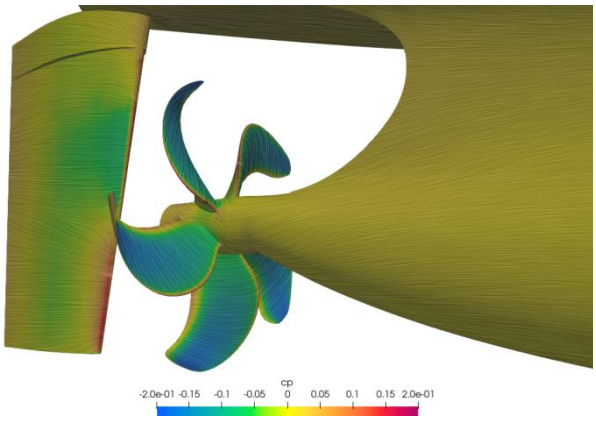

Figure 7: C_p-distribution and limiting stream lines on aft ship and unconventional propeller P3590

Table 3 shows the relevant efficiencies by means of different approaches for the stock propeller (P3509) as well as for the designs with negative- and positive tip-rake respectively. Here EFD-BEM stands for the resistance- and stock propeller propulsion test results (EFD) combined with BEM POW results, CFD-CFD holds for the full RANS propulsion analysis whereas EFD-EFD stands for complete model test results finally performed.

Related to the stock propeller both numerical approaches show a gain in propulsive efficiency η_D of 2.2% to 3.3% for the negative tip-rake version and 1.5% to 1.9% for the positive tip-rake propeller. On this basis it was decided to manufacture the negative tip-rake propeller P3590 for further model test investigations.

It should be mentioned that this relation between negative- and positive tip-rake designs holds for this project and should not be understood as a general tendency.

The model test results with this unconventional propeller design P3590 revealed still an efficiency gain in η_D of 1.5% and in behind efficiency $\eta_B = \eta_0 * \eta_R$ of 1.7% but unfortunately less than expected (3.3% or 2.2%).

Table 3: Propulsion Prediction, Service Condition, Design Speed

method	prop.	η_B	η_H	η_D	$\Delta\eta_D$ %
EFD-BEM	stock	0.705	1.079	0.761	**0.0%**
EFD-BEM	neg-rake	0.728	1.079	0.786	**3.3%**
EFD-BEM	pos-rake	0.716	1.079	0.772	**1.5%**
CFD-CFD	stock	0.705	1.045	0.736	**0.0%**
CFD-CFD	neg-rake	0.722	1.042	0.752	**2.2%**
CFD-CFD	pos-rake	0.719	1.043	0.750	**1.9%**
EFD-EFD	stock	0.705	1.053	0.742	**0.0%**
EFD-EFD	neg-rake	0.717	1.051	0.753	**1.5%**

For the stock propeller the model tests led to the same η_B as the full RANS analysis whereas for the design propeller it is 0.7% lower than predicted. Due to higher complexity the unconventional propeller has been predicted with less accuracy than the stock propeller, but at the end it is still a promising result, encouraging us in continuing the development in this direction.

A propeller for such a container vessel has a thrust loading coefficient c_{th} of about 0.9, which seems to be a difficult starting point for such applications. For propellers with higher thrust loading coefficient c_{th} the induced losses are higher and the possible efficiency gain for such tip-raked propellers could be higher as well.

3.2 Influence of TE Geometry onto Propeller Characteristics

The shape and the discretization of a propeller leading edge gain most probably reasonable attention during CFD analyses. Since the original shape of the anti-singing edge is usually not accounted in the CFD model, the question arises how to discretize the trailing edge (TE) for design predictions. This means that the profile shape near the TE can be handled in different manners according to experience. Accounting for the real flow behavior near the original TE by means of RANS would lead to much higher effort than believed to be affordable for design predictions.

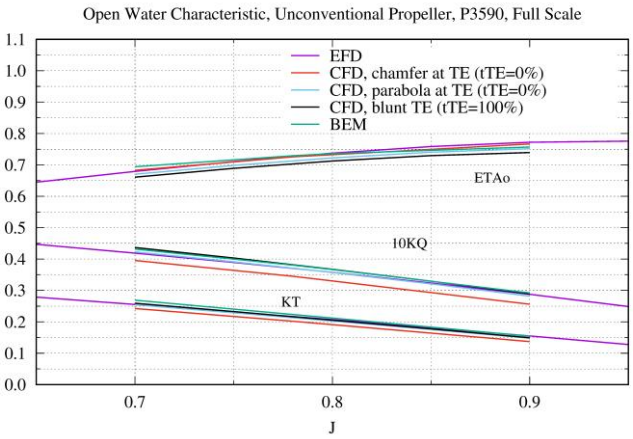

Figure 8: Open water characteristic, unconventional propeller, P3590

Figure 8 shows the influence of the modelled trailing edge thickness onto the POW results of the unconventional propeller P3590 in full scale. The red curve shows the results related to introducing simply a symmetrical chamfer towards zero thickness (t_{TE}=0%) starting from 95% chord. The idea is to introduce less or even no separation behind the TE, which might not be handled accurately by RANS design predictions. This leads to artificial curvature near 95% chord on the back as well as on the face side with correspondingly low pressure creating low thrust coefficient K_T and torque coefficient K_Q. Due to the symmetrical pressure related error on back- and on face side the efficiency η_0 is met very well, compared at constant J.

The blue curve corresponds to a local thickness modification starting also from 95% chord to zero thickness (t_{TE}=0%) by a parabola. This introduces a local but therefore larger curvature near the TE and correspondingly local separation and corresponding drag. Practically speaking the K_T and K_Q are met sufficiently well but to a slightly lesser degree it holds for η_0. The former described pressure field related inaccuracy is avoided by the price of separation at the TE.

For the original design profile geometry with blunt TE stands the black curve (t_{TE}=100%), where no artificial curvature but separation at the TE is introduced. The K_T is met but not K_Q as well as η_0.

A BEM code like PPB is not as sensible to trailing edge details, since the thickness will be automatically set to zero and separation is naturally not part of the solution. The way how the trailing edge of the blades is discretized seems to be crucial for the detailed assessment with finite volume modeling (RANS) rather than for BEM code analysis, even more for ice propellers with thicker trailing edges than for open water propellers.

Near the design advance coefficient (J=0.78) the results of the BEM code are close to the RANS and the experimental results. For conventional propellers this is

already part of experience, but for unconventional propellers these are promising news.

Currently HSVA implements a RANS-BEM coupling between the PPB BEM code and FreSCo^{+}. This is expected to allow RANS-BEM propulsion predictions even for unconventional tip-rake propellers with good accuracy by lower effort compared to a full RANS-RANS approach.

3.4 Propeller Paint Test Results

Propeller paint tests in open water as well as in behind condition at different Rn's have been performed to investigate the limiting stream lines in the boundary layer at model scale. Out of these results two examples are shown in Figures 9 and 10 for the stock- and the design tip-rake propeller respectively in POW condition.

N=20Hz, Rn=8.076E5, J=0.780

Figure 9: Limiting stream lines on back (top) and face side (bot), P3509

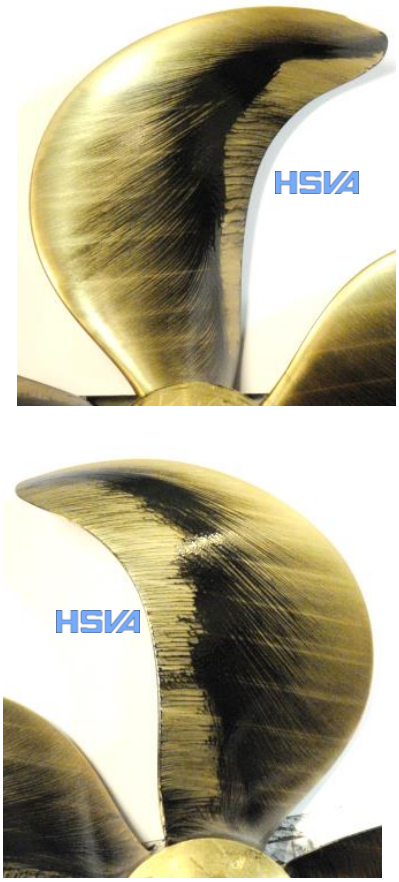

N=19Hz, Rn=7.35E5, J=0.788

Figure 10: Limiting stream lines on back (top) and face side (bot), P3590

Even for the large Rn's of 7.4E5 and 8.1E5 laminar flow dominates the back side of both propellers. The paint traces or limiting stream lines show a radially deviated orientation from the leading edge towards the tip, where the paint is finally washed out. The location of a laminar separation bubble (LSB) near 85% chord is visible by means of the accumulated paint, where hardly any tangential friction force exists but a centrifugal force transporting the paint radially outwards. Behind the LSB the flow is attached again and transition to turbulence takes place.

For the stock propeller P3509 the LSB changes near the tip the path in chord wise direction since it hits a region of turbulent flow. According to this path the flow within the boundary layer and most probably the tip vortex seem to leave the blade tip parallel to the moving direction.

To a large amount the paint traces on the back side of P3590 (Figure 10) show a similar orientation. The LSB shows a wider chord wise extent which is related to the higher t/c ratio of the blade.

Further the path of the LSB at the tip shows a less chord wise orientation compared to P3509 suggesting a different path of the flow and the corresponding tip vortex.

The reasons for the different orientation of the limiting stream lines near the tip can be manifold. The laminar

flow on face side even near the tip of P3590 will have an influence onto the vortex roll-up. Further the different radial load distribution might change the development of the boundary layer and the path of the tip vortex. Last but not least the aforementioned positive pitch angle ϕ_w changes intentionally the chord wise as well as radial load distribution. The latter suggests a lower radial contraction of the slip stream compared to conventional designs.

The face side of P3509 shows above a critical radius of 0.75R traces from turbulent flow right from the start of the leading edge. Below the critical radius transition to turbulent flow occurs w/o a visible LSB. To the contrary the unconventional propeller P3590 shows a wide LSB on face side which is visible from the hub towards to the tip. This difference of paint traces is related to the larger thickness to chord ratio t/c and larger pitch ratio P/D of the unconventional propeller P3590 related to the conventional one.

3.5 Cavitation Behavior

Figures 11 and 12 show exemplarily the cavitation pattern on the back side of both propellers at a blade position of 200° which represents 20° beyond the 12:00 position. The corresponding pressure pulses of both propellers together with statistical results for similar vessels are found in Figure 13.

Interestingly the first harmonic of the unconventional design is not higher than of the stock propeller and both are lower than acc. to statistic. Here the strong and stable tip vortex and concentrated sheet cavitation near the tip is expected to be the driving source of this result. Related to statistics the pressure pulses are fine, but nevertheless it would be beneficial to reduce the amplitudes of the tip rake propeller P3590 at the second harmonic.

As mentioned before the stock propeller P3509 is tip unloaded to the contrary of P3590 (see Figure 4). Interestingly both propellers behave similar in terms of sheet cavitation and pressure pulses at least at the first blade harmonic.

The second harmonic amplitude of P3590 is most probably related to the sheet cavity which appears relatively thick near the trailing edge. This is prone to induce a pressure peak by means of the collapsing process. Due to the very stable tip vortex cavitation no bursting phenomena were observed which would have caused pressure pulses at higher harmonics.

Interestingly the path of the cavitating tip vortex shows directly behind the blade less slip stream contraction for the tip-rake propeller than for the conventional one.

The lower blade area ratio of the design propeller seems not to have a drawback in this respect. The aim to reduce the amount of sheet cavitation extent by concentrating the load towards the tip as well as stabilizing the tip vortex worked well.

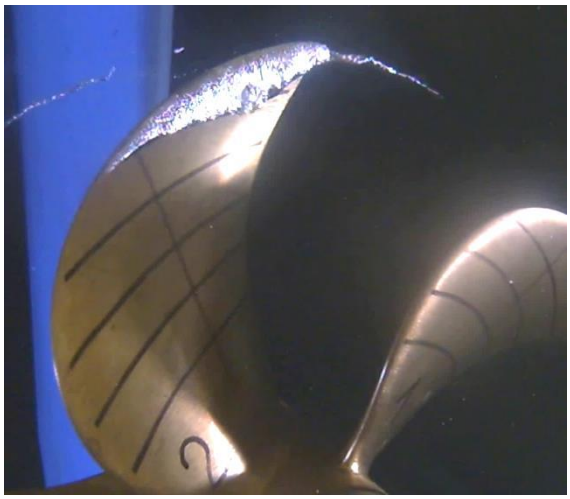

Figure 11: Video frame, conventional propeller P3509

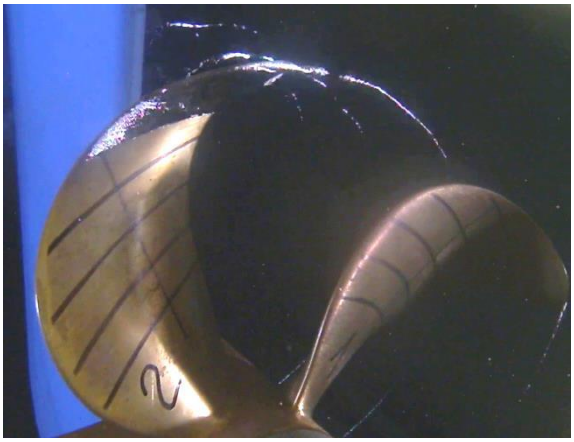

Figure 12: Video frame, unconventional propeller P3590

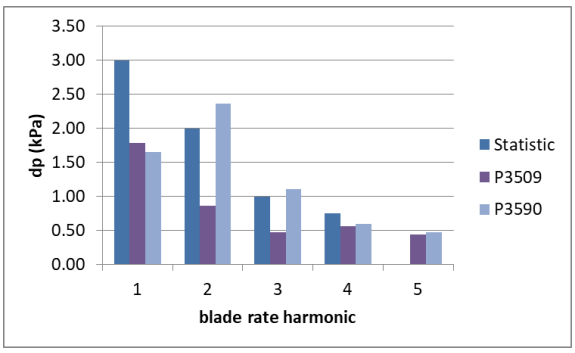

Figure 13: Pressure pulses 1st - 5th harmonic, P3509 conventional, P3590 unconventional)

4 CONCLUSION

This paper summarizes recent developments at HSVA in unconventional propeller design and its subsequent analyses and model tests.

Both positive- and negative tip-rake propellers have been designed and investigated numerically. Some experience regarding these unconventional propeller shapes have been shared.

By means of different propulsion prediction methods an efficiency potential versus reference propeller of 1.9% and 3.3% for the positive- and negative tip-raked propeller respectively has been predicted. On this basis the negative tip-rake propeller has been manufactured and tested.

Model test results revealed an efficiency gain in η_D of 1.5% for the negative tip-raked propeller. The main difference is related to a gain in η_B and to a lesser extent in η_H.

The reason for the lower efficiency gain can be manifold:

First due to higher complexity the unconventional propeller has been predicted with less accuracy than the stock propeller, but at the end it is still a promising result, encouraging us in continuing the development in this direction.

Second the possible efficiency gain is practically more difficult to obtain when the induced losses are low (c_{th}=0.9) like for the actual case.

The influence of the way how the trailing edge is discretized has been shown, which seems to be crucial for the detailed assessment with finite volume modeling (RANS) rather than for BEM code analysis.

The aim to reduce the amount of sheet cavitation extent by concentrating the load towards the tip as well as stabilizing the tip vortex worked well from the cavitation and pressure pulses point of view.

ACKNOWLEDGEMENT

This work is based on fruitful contributions from several colleagues at HSVA, as there are Katrin Lassen, Julia Schmale, Hilmar Klug, Johannes Strobel, Lars Koopmann and Björn Carstensen.

The financial support of the research project DeffProForm (FKZ 03SX516D) by the German ministry (BMWK) Bundesministerium für Wirtschaft und Energie represented by Projektträger Jülich (PTJ) is gratefully acknowledged.

REFERENCES

Andersen, P. et al.: (2002), 'Development and Full-Scale Evaluation of a New Marine Propeller Type', 97th Hauptversammlung der Schiffbautechnischen Gesellschaft, Hamburg, November 2002

Brown, M. et al.: (2014), 'Improving Propeller Efficiency Through Tip Loading', 30th Symposium on Naval Hydrodynamics, Hobart. Australia, 2-7 November 2014

Gaggero, S. et al.: (2015), 'A Design by Optimization of Tip Loaded Propellers', Fourth International Symposium on Marine Propulsors, SMP'15, Austin, Texas, USA, June 2015

Hafermann, D.: (2007), "The new RANSE Code FreSCo for Ship Application", STG Jahrbuch

Johannsen, C.: (2018), "Propulsion Testing in the HYKAT Cavitation Tunnel", A Yücel Odabaşi Colloquium Series, Istanbul

Lücke, T., Streckwall, H.: (2017), "Experience with Small Blade Area Propeller Performances", SMP'17, Espoo, Finland, June 2017

Lücke, T.: (2019), "Particular Model Propeller Behavior in EFD & CFD", SMP'19, Rome, Italy, May 2019

Müller, J.: (2017), "HYTES – HYKAT Tested Energy Saving Devices", 5th Int. Conf. on Advanced Model Measurement Technology for the Marine Industry (AMT'17), Glasgow, UK, 2017

Schumacher A. (2020), "Weiterentwicklung der Harmonisch-Erregte-Rollschwingung-Methode zur Bestimmung der Rolldämpfung und der Propulsionsleistung von Schiffen (HERMes)", HSVA-Report No. 1695, Förderkennzeichen 03SX413A, 2020

Streckwall, H. (2000). „Propeller-Kavitation und propellererregte Druckschwankungen auf der Basis eines potentialorientierten Randelemente-Verfahrens", HSVA Bericht Nr. 1639, 2000